JOURNAL OF GEOPHYSICAL RESEARCH, VOL. 111, D12314, doi:10.1029/2005JD006490, 2006

Deep convective influence on the Asian summer monsoon anticyclone and associated tracer variability observed with Atmospheric Infrared Sounder (AIRS)

William J. Randel[1] and Mijeong Park[1]

Received 12 July 2005; revised 7 November 2005; accepted 2 March 2006; published 27 June 2006.

[1] The Asian summer monsoon anticyclone is linked to climatological deep convection over Southeast Asia, and the coupling of circulation and convection strongly influences constituent behavior in the upper troposphere – lower stratosphere (UTLS). This work explores the variability of the Asian monsoon circulation and trace constituents linked to transient deep convection, on the basis of dynamical fields and outgoing longwave radiation (OLR) data, plus water vapor and ozone retrievals from the Atmospheric Infrared Sounder (AIRS) instrument. Within the monsoon region, transient deep convection varies with a timescale of ~10–20 days, linked to active/break cycles in the monsoon circulation. We show that these convective events trigger variations of the anticyclone itself, with strong correlations between OLR and the area of low potential vorticity (PV) defining the anticyclone. Relatively high PV (stratospheric air) is also advected to low latitudes to the east of the anticyclone following enhanced convection. AIRS data show that the transient convective events are associated with the vertical transport of low ozone and high water vapor into the UTLS region, with significant effects over potential temperature levels 340–360 K (~7–13 km). Idealized transport calculations are used to demonstrate that constituent anomalies are confined within the upper tropospheric anticyclone, and this confinement contributes to the climatological constituent patterns observed during summer.

Citation: Randel, W. J., and M. Park (2006), Deep convective influence on the Asian summer monsoon anticyclone and associated tracer variability observed with Atmospheric Infrared Sounder (AIRS), *J. Geophys. Res.*, *111*, D12314, doi:10.1029/2005JD006490.

1. Introduction

[2] The Asian summer monsoon is a dominant climatological feature of the global circulation during Northern summer (~June to September). The monsoon circulation consists of cyclonic flow and convergence in the lower troposphere together with strong anticyclonic circulation and divergence in the upper troposphere. This circulation is coupled with persistent deep convection over the south Asia region during summer, and *Hoskins and Rodwell* [1995] have shown that the climatological monsoon structure is primarily a response to diabatic heating associated with the convection. The upper tropospheric anticyclonic circulation extends into the lower stratosphere; the monsoon tropopause is relatively high and cold [*Highwood and Hoskins*, 1998], with frequent occurrence of cirrus clouds [*Wang et al.*, 1996].

[3] In addition to the strong dynamical signature in the upper troposphere, the influence of the monsoon is also evident in chemical constituents. In fact, constituent fields throughout the upper troposphere–lower stratosphere (UTLS) region often exhibit a monsoon signature during summer. For example, within the monsoon anticyclone UTLS water vapor is relatively high [*Rosenlof et al.*, 1997; *Jackson et al.*, 1998], ozone is relatively low [*Randel et al.*, 2001], and methane, nitrogen oxides [*Park et al.*, 2004], and carbon monoxide [*Li et al.*, 2005a, 2005b] are relatively high. However, the mechanism(s) that maintain these climatological features, or their detailed synoptic variability, are not well known. The monsoon circulation also probably plays an important role in stratosphere-troposphere exchange (STE) during summer [*Dethof et al.*, 1999; *Bannister et al.*, 2004; *Gettelman et al.*, 2004a].

[4] The monsoon is not a steady circulation but exhibits substantial intraseasonal variability, often referred to as active/break cycles. These cycles are evident as coupled oscillations of circulation and deep convection within the monsoon region, and observational studies have identified oscillations with timescales 10–20 and 30–60 days [*Krishnamurti and Bhalme*, 1976; *Annamalai and Slingo*, 2001, and references therein]. The 30–60 day (or 40-day) mode is associated with northward propagation of convection, often during the onset phase of the monsoon [e.g., *Yasunari*, 1981], whereas the 10–20 day mode is a westward propagating feature that is prominent during the mature phase of the monsoon [e.g., *Krishnamurti and Ardanuy*, 1980]. In addition to these convectively coupled modes, *Hsu and Plumb* [2000] have studied the behavior of

[1]National Center for Atmospheric Research, Boulder, Colorado, USA.

0148-0227/06/2005JD006490$09.00

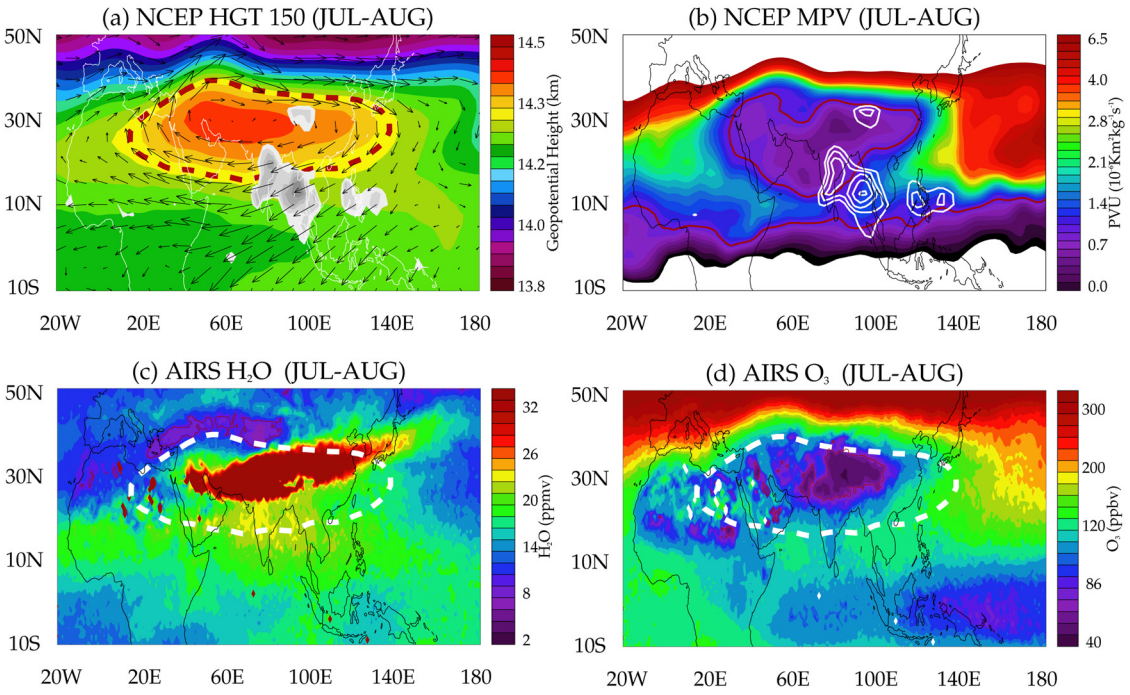

Figure 1. Horizontal structures of 2-month (July and August 2003) average (a) National Centers for Environmental Prediction (NCEP) geopotential height (km) and horizontal winds (m s^{-1}) at 150 hPa, (b) modified potential vorticity (MPV) (PVU, 10^{-6} Km^2 kg^{-1} s^{-1}), (c) Atmospheric Infrared Sounder (AIRS) water vapor (ppmv), and (d) ozone (ppbv) centered in Asian monsoon region at 360 K. White contours in Figures 1a and 1b show the OLR less than or equal to 205 (W m^{-2}). Thick dotted lines in Figures 1a, 1c, and 1d mark the 14,320 m geopotential height contour.

an idealized monsoon anticyclonic circulation and find dynamic instability leading to periodic shedding of secondary anticyclones. Evidence suggesting eddy shedding in observational data was shown by *Popovic and Plumb* [2001].

[5] The objective of our work is an observational study of dynamical and constituent variability of the Asian monsoon anticyclone and its coupling to transient deep convection. We analyze daily variability of dynamical fields and outgoing longwave radiation (OLR) measurements (as a proxy for deep convection), together with ozone and water vapor measurements from the Atmospheric Infrared Sounder (AIRS) instrument. The OLR data reveal strong variations associated with the monsoon active/break cycles discussed above, and these variations in convection are evident in the monsoon dynamical and constituent fields. We use this variability to characterize the influence of transient convection on circulation and transport within the monsoon, and understand the processes that contribute to maintenance of the climatological behavior discussed above. The observations suggest that constituents are confined in the upper troposphere by the strong anticyclonic circulation, and we include some idealized transport calculations within the monsoon region to quantify this behavior.

2. Data and Analyses

2.1. Meteorological Data

[6] The meteorological data and some relevant dynamical calculations are briefly described here. Temperature and three dimensional wind fields are obtained from the National Centers for Environmental Prediction/National Center for Atmospheric Research (NCEP/NCAR) reanalysis pressure level data, with 2.5° × 2.5° horizontal resolution [*Kalnay et al.*, 1996]. From these data we derive potential vorticity (PV) fields, following standard calculations [*Andrews et al.*, 1987]. Because we wish to analyze PV over a range of altitudes, we use a modified potential vorticity (MPV) from *Lait* [1994]. MPV reduces the exponential variability of PV with height by applying a scaling factor, which is a function of potential temperature (θ), and is defined as MPV = $PV(\theta/\theta_0)^{-9/2}$, with θ_0 a reference potential temperature (400 K). We calculate MPV from the NCEP/NCAR reanalysis data and interpolate to isentropic levels.

[7] As a measure of the overall strength of the monsoon anticyclonic flow, we also calculate the circulation along a constant contour of geopotential height (as an approximation to a material streamline). Circulation (C) is defined as

$$C \equiv \oint \mathbf{U} \bullet d\mathbf{l} = \oint (\mathbf{u}dx + \mathbf{v}dy), \qquad (1)$$

where **U** is a velocity vector locally tangent to the contour **l** [*Holton*, 2004, chap. 4]. The circulation is calculated along a closed contour of geopotential height, chosen such that the associated streamline is near the wind maximum in the upper troposphere. We choose the 14,320 m geopotential height contour on the 150 hPa pressure surface (red dashed lines shown in Figure 1a), which exists as a closed contour every day during Northern summer after early May. We note that the circulation C is equal to the area integrated relative vorticity within the contour via Stokes' theorem [*Holton*,

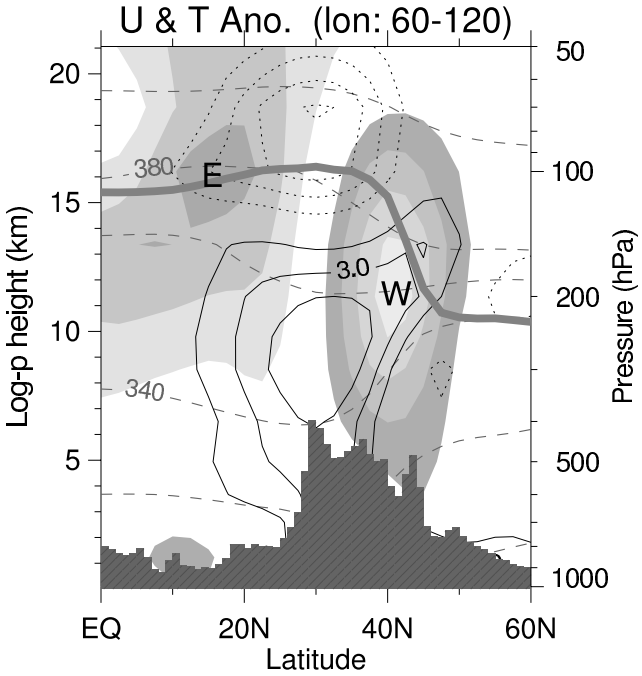

Figure 2. Vertical structures of 2-month (July and August) average NCEP zonal wind (shaded) and temperature anomalies (thin lines) averaged in 60°–120°E longitudes. The westerly and easterly jets are shaded separately and denoted by "W" and "E," respectively. The shaded contours are at intervals of 8 m s^{-1}; the maximum westerly winds are near 36 m s^{-1}, and the maximum easterlies near 31 m s^{-1}. The temperature anomaly contours are ±1.5, 3.0, and 4.5 K, shown as solid (positive) and dotted (negative) lines, respectively. Dashed lines denote isentropic surfaces (320, 340, 360, 380, and 450 K), and thermal tropopause from NCEP/NCAR reanalysis is noted by a thick solid line. The regional topography is added at the bottom.

2004]. Because the relative vorticity is related to the PV (MPV) field, it is reasonable that variations in circulation (on a pressure surface) are closely linked to the area of low MPV on nearby isentropes (as shown below); thus these are complementary but closely related diagnostics.

[8] We use OLR as a measure of deep convection in the monsoon region. Daily interpolated OLR data is obtained by the NOAA-CIRES Climate Diagnostics Center (http://www.cdc.noaa.gov). These data are discussed in detail by *Liebman and Smith* [1996].

2.2. AIRS Ozone and Water Vapor

[9] Vertical profiles of water vapor and ozone mixing ratios are obtained from AIRS measurements. AIRS is one of six instruments on board the NASA Aqua spacecraft, and has been operational since September 2002 [*Aumann et al.*, 2003]. In this work we focus on the Northern summer (May to September) of 2003. We use AIRS level 3 retrieval products on a 1° × 1° grid, with missing data filled by interpolation [*Renka*, 1982]. The water vapor and ozone retrieval products are available on 12 standard pressure levels over 1000–100 hPa, with data on each pressure level representing the layer mean between adjacent levels. For some diagnostics we have interpolated the AIRS pressure level data to isentropic levels. Validation of the AIRS water vapor retrieval (an operational product) is discussed by *Hagan et al.* [2004]; the AIRS ozone retrieval is a research product that is currently undergoing validation. *Gettelman et al.* [2004b] have compared AIRS retrievals with research aircraft measurements in the UTLS region; their limited comparisons suggest that the AIRS water vapor is within ±25% of aircraft observations for mixing ratios above 10 ppmv, and AIRS ozone has a ∼30% positive bias in the upper troposphere but can reasonably track variability over a range of mixing ratios from approximately 50–500 ppbv.

3. Monsoon Climatological Structure

[10] Climatological structure of the south Asian monsoon anticyclone is shown in Figure 1, based on a 2-month

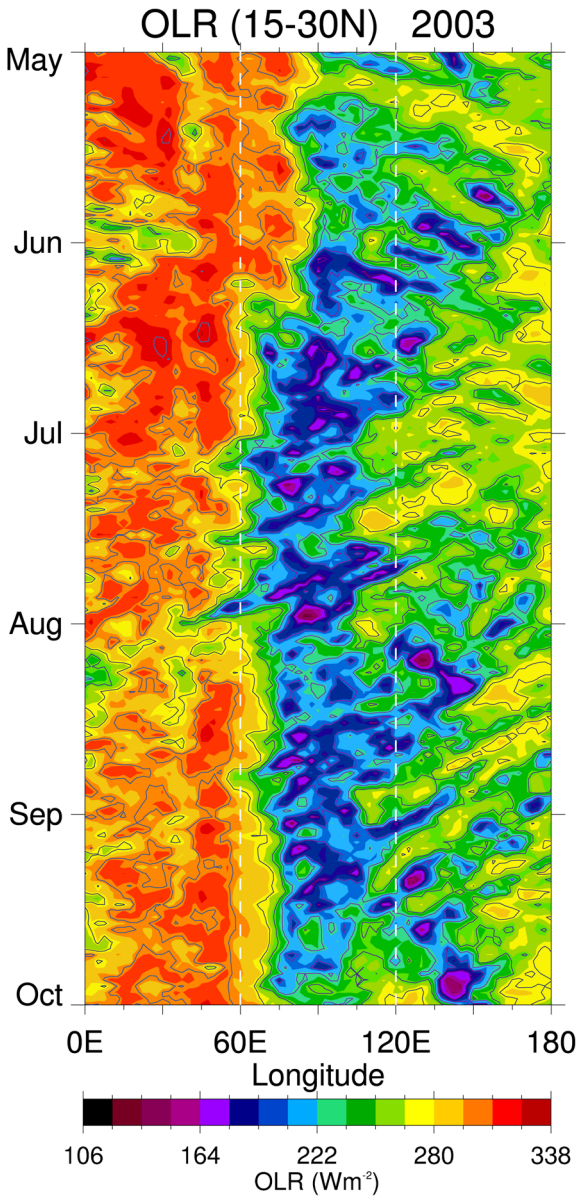

Figure 3. Hovmöller diagram of outgoing longwave radiation (OLR) (W m^{-2}) averaged over 15°–30°N from May to September 2003.

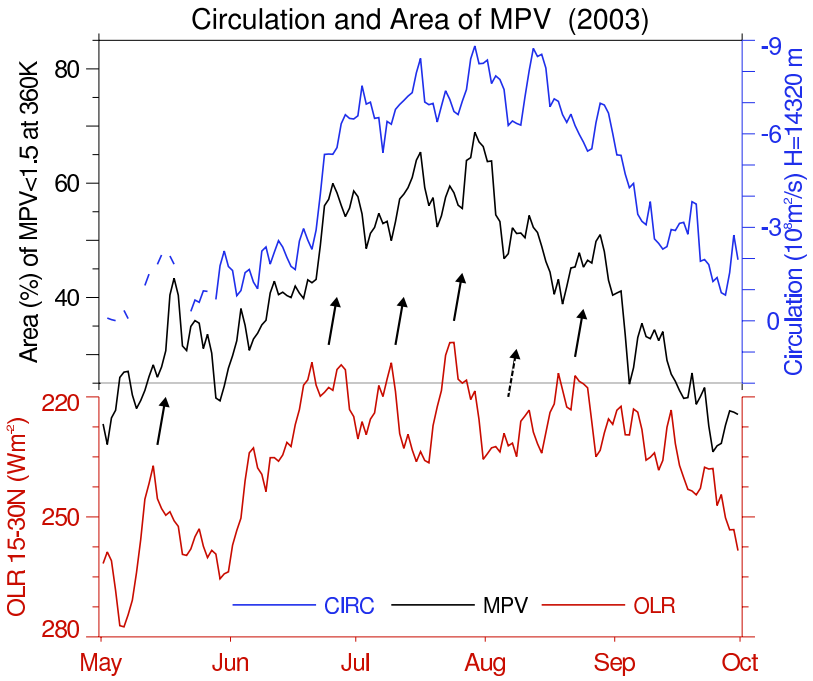

Figure 4. Bottom (red) curve shows OLR reference time series, averaged over 15°–30°N and 60°–120°E. Black line shows area of MPV less than 1.5 PVU at 360 K, as a fraction (%) of the region 20°–40°N and 20°–140°E. Blue line shows time series of circulation (equation (1)) in the anticyclone at 150 hPa. Arrows denote episodes of enhanced deep convection and associated changes in intensity of the anticyclone.

average during the mature phase (July and August, 2003). The dynamical structure is shown by two diagnostics: the 150 hPa geopotential height and horizontal winds (Figure 1a) and the 360 K MPV (Figure 1b). A strong anticyclonic circulation is evident in Figure 1a, and this is associated with relatively low MPV over the region ∼15°–35°N and ∼40°–120°E in Figure 1b. We consider (1) the circulation around the anticyclone (equations (1)) and (2) the area of low MPV as identifying the strength of the anticyclone. The time variability of these two quantities is discussed below. Figures 1a and 1b also indicate the location of time-averaged deep convection (low OLR) for July and August 2003. The time-averaged deep convection is not co-located with the center of the anticyclone but rather lies in the southeast quadrant.

[11] Aspects of the vertical structure of the time average monsoon circulation are shown in Figure 2. This shows a zonal slice, averaged over longitudes 60°–120°E, of the zonal winds and potential temperatures, the tropopause, and the local temperature anomalies (deviations from the zonal mean). The balanced structure in Figure 2 shows the monsoon circulation has a warm core up to ∼13 km, overlaid by cold anomalies in the lower stratosphere; the monsoon tropopause is relatively high and cold near 30°N. The westerly jet on the northern flank of the monsoon extends from near the surface to the lower stratosphere, with a core near 12 km. In contrast, the easterly jet on the equatorial side is centered substantially higher (∼16 km); these monsoon easterlies extend into the stratosphere, and merge with the climatological summer easterly winds. During NH summer in 2003, the equatorial quasi-biennial oscillation (QBO) was in a weak easterly phase in the lower

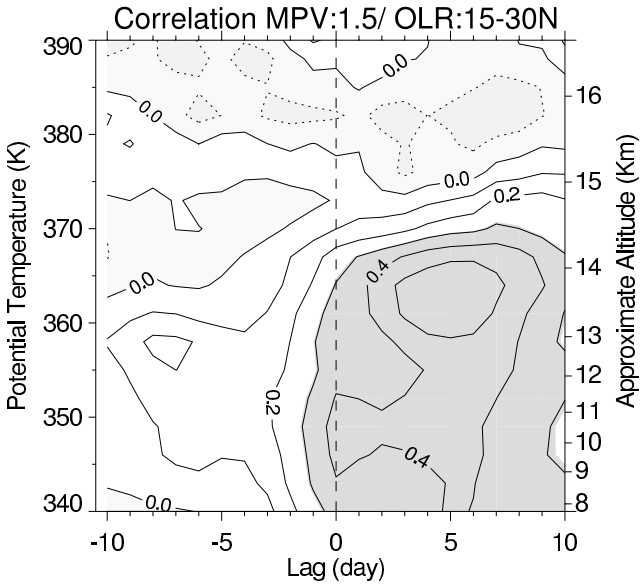

Figure 5. Lag correlations between the OLR reference time series (Figure 4) and the area of MPV (≤1.5 PVU) on different potential temperature levels. Calculations are for June and August 2003. Contour interval is 0.1. The 5% significance level for these correlations, evaluated using a resampling technique [*Efron and Tibshirani*, 1993], is near 0.3.

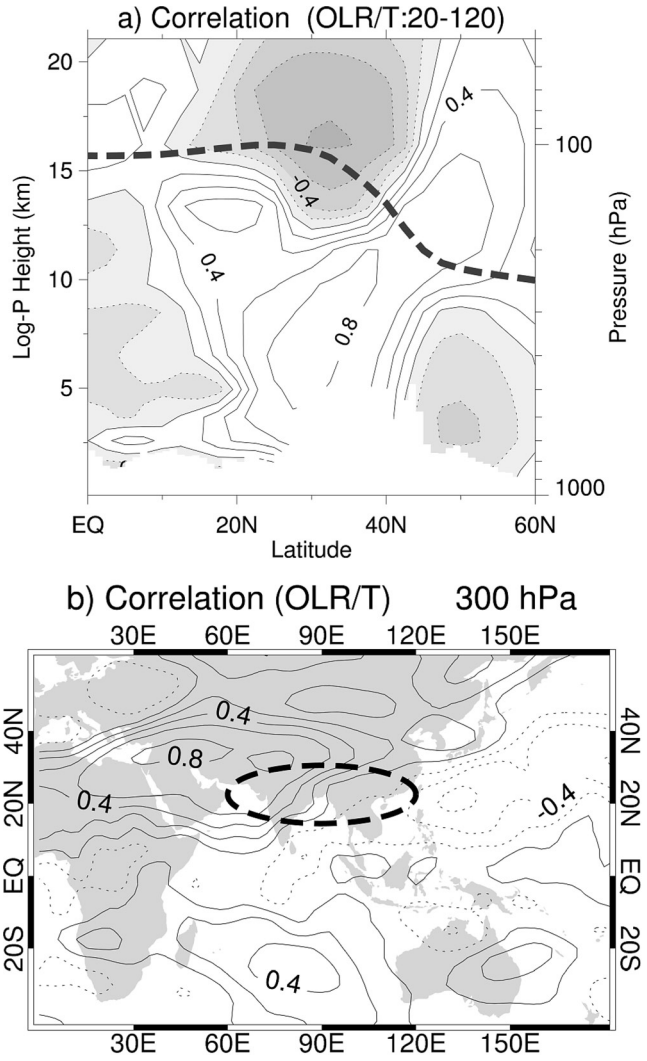

Figure 6. (a) Correlation between OLR proxy time series for monsoon convection and temperature anomalies averaged over longitudes 20°–120°E, calculated for May to September, where the dashed line denotes the tropopause. (b) Correlation between OLR reference time series (representing the region denoted by the heavy dashed line) and temperature at 300 hPa.

stratosphere. In terms of strong winds that act to restrict meridional tracer transport [e.g., *Haynes and Shuckburgh*, 2000; *Bowman*, 2006], the time mean structure in Figure 2 suggests that the monsoon winds may provide effective containment over altitudes spanning the upper troposphere to lower stratosphere (~10–16 km). This vertical range is confirmed in our transport calculations discussed in section 6.

[12] The time-averaged structure of upper tropospheric water vapor and ozone derived from AIRS data are shown in Figures 1c and 1d, calculated for the 360 K isentropic level. These figures also show the location of the upper tropospheric anticyclone, denoted by the 14,320 m contour of the 150 hPa geopotential height (from Figure 1a). Water vapor (Figure 1c) shows high values within the core of the anticyclone, with the maximum values extending to the northeast (following the westerly winds near 40°N). Ozone shows relatively low values over the anticyclonic region, with a clear minimum near the center (~30°N, 80°E). We note that the extrema for both water vapor and ozone in Figure 1 are not co-located with the time-averaged deep convection (low OLR values shown in Figures 1a and 1b) but rather with the overall circulation patterns, and in particular with the region of low MPV.

4. Variability and Coupling to Convection

[13] Our focus here is to understand the coupling of transient deep convection (associated with the active/break spells of the monsoon) with the monsoon temperatures, anticyclonic circulation, and upper troposphere tracer variability. Figure 3 shows a Hovmöller diagram of OLR over 15°–30°N during May to September 2003, which highlights variability of deep convection within the monsoon region. Deep convection (low OLR in Figure 3) exhibits fluctuations on timescales of ~5–20 days, with some eastward propagation during May to June, followed by westward propagation over this latitude range during July to September. This transience follows evolution of the upper tropospheric zonal winds in this latitude band, which become easterly (see Figures 1a–2) after the middle of June. The OLR variability in Figure 3 is consistent with the 10–20 day active/break monsoon periods identified in previous studies [e.g., *Krishnamurti and Ardanuy*, 1980; *Fujinami and Yasunari*, 2004]. In order to quantify the strength of convective forcing, we use an average of OLR over 15°–30°N and 60°–120°E as a proxy for monsoon convection in the rest of this work. This is a subjective choice, based on overall correlations with various dynamical and tracer variations. We note a large convective event occurs over longitudes ~120°–150°E (outside of our averaging area) during August 3–12 in Figure 3; while this event also influences the monsoon circulation and constituents, we find the 60°–120°E average to be the best overall proxy.

[14] Time series of the monsoon convection proxy over May to September 2003 is shown in Figure 4, together with two diagnostics of the upper tropospheric anticyclonic flow: (1) the circulation (equation (1)) evaluated along the 14,320 m geopotential height contour at 150 hPa, and (2) the area of low MPV on the 360 K isentrope (specifically, the area of MPV $\leq$1.5). As discussed above, these diagnostics are related (stronger anticyclonic circulation is associated with increased area of low MPV) but provide complementary information. The monsoon convection and circulation diagnostics in Figure 4 show similar seasonal variability, with maxima during late June to August. More importantly, the circulation diagnostics exhibit ~10–20 day fluctuations that are coupled to the variations in convection; there are five events highlighted by arrows in Figure 4, plus a sixth in early August associated with the convective event over 120°–150°E discussed above. There is an apparent time lag between the OLR maxima and the circulation changes, such that the maximum circulation effects occur ~5 days after the convective maxima. The relationship between OLR and area of low MPV over a range of isentropic levels is quantified in Figure 5, showing the correlation as a function of altitude (potential temperature) and time lag. Significant correlations are found over theta levels ~340–370 K

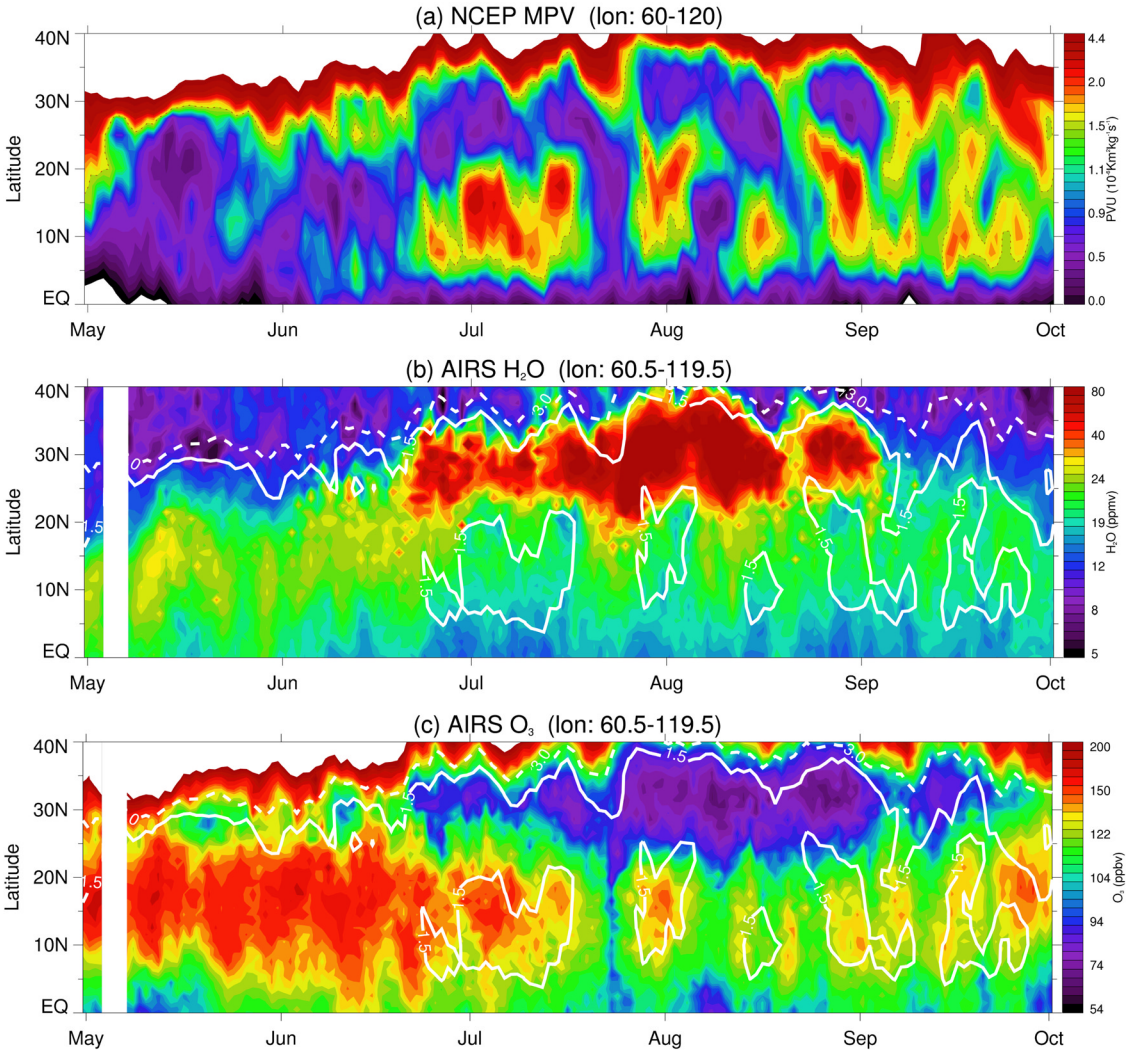

Figure 7. Time and latitude sections of (a) MPV (PVU), (b) AIRS water vapor (ppmv), and (c) ozone (ppbv) averaged over 60°–120°E on the 360 K isentrope (May to September 2003). The white solid contours overlaid on the AIRS data show MPV contours of 1.5 (solid) and 3.0 (dashed) PVU.

(altitudes ~8–14 km), with maximum values near time lag 5 days (convection preceding low MPV area). This time lag is consistent with convective-associated diabatic heating in the middle troposphere being an important component for the UTLS potential vorticity tendency equation [*Andrews et al.*, 1987]; that is, the PV itself responds as an integral to the episodic forcing.

[15] Variations in deep convection are also correlated with tropospheric and lower stratospheric temperatures throughout the monsoon region. Figure 6a shows correlations between temperature anomalies (deviations from the zonal mean) over 20°–120°E and the OLR convection proxy (lower curve in Figure 4) during May to September. Strong positive (negative) correlations are found for temperatures in the middle troposphere (lower stratosphere), and these patterns reflect the climatological mean temperature structure seen in Figure 2. Together with the fluctuations in anticyclonic circulation seen in Figure 4, this demonstrates that the entire balanced anticyclonic circulation varies in concert with transient deep convection. The horizontal structure of upper tropospheric (300 hPa) temperature fluctuations coherent with deep convection (OLR proxy) is shown in Figure 6b. The strongest correlations (near 0.8) occur over the broad monsoon region extending from 20°–100°E and 15°–40°N. This temperature response is significantly northwest of the region of strong monsoon convection (as illustrated in Figure 6b), but this structure is consistent with the expected response to low-latitude heating centered off the equator [*Gill*, 1980; *Hoskins and Rodwell*, 1995; *Dima et al.*, 2005]. Note there is also a symmetric temperature response observed in the Southern Hemisphere subtropics in Figure 6b (over ~60°–100°E and 15°–40°S), consistent with such a dynamical response to off-equatorial low-frequency forcing.

[16] Time and latitude variations of MPV, water vapor and ozone over the central monsoon region (60°–120°E) at 360 K are shown in Figure 7. In Figure 7a, episodes of low MPV are observed over ~20°–35°N throughout the summer, following the deep convective events in lower latitudes (15°–30°N) in Figure 4. For events during the mature phase (late June to August), the low MPV regions in midlatitudes are accompanied by relatively high MPV in low latitudes

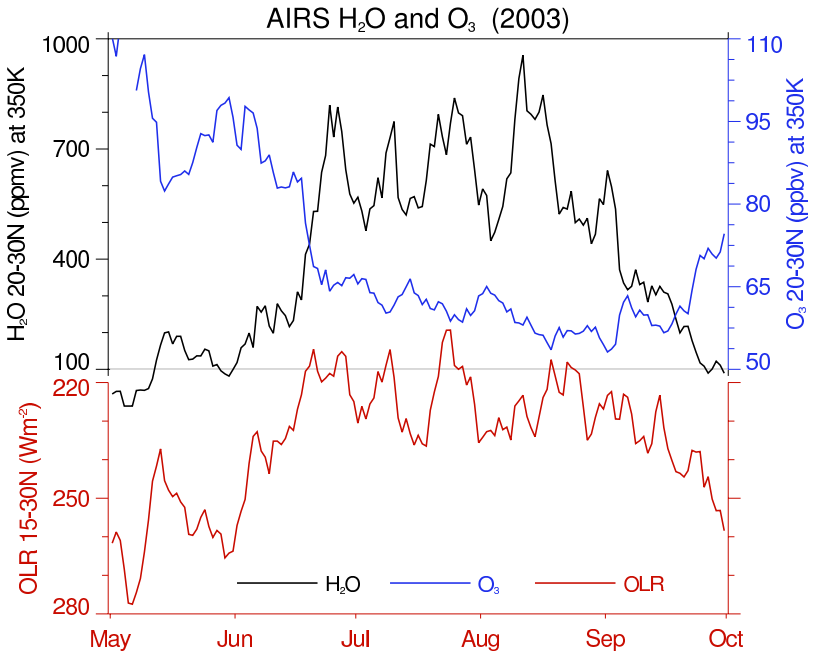

Figure 8. Time series of AIRS water vapor (ppmv) and ozone (ppbv) averaged over 20°–30°N and 60°–120°E at 350 K, together with the OLR reference time series. (Red curve is the same as in Figure 4.)

(equatorward of 20°N), so that there is a north-south dipole structure in MPV. These low-latitude maxima are related to anticyclonic advection of high MPV (stratospheric air) on the east side of the monsoon region, as discussed further below.

[17] The corresponding time sections of AIRS water vapor and ozone in the monsoon region are shown in Figures 7b and 7c, with MPV values of 1.5 and 3.0 PVU (from Figure 7a) overlaid as white contours. These time series show the development of high water vapor and low ozone within the monsoon region (over latitudes ~20°–35°N), with extrema during late June through August. Variations in both water vapor and ozone are closely linked to changes in MPV, both within the central monsoon region (latitudes ~20°–35°N), and also over lower latitudes (equatorward of 20°N). Ozone in particular exhibits episodic north-south dipole patterns very similar to MPV. It is noteworthy that MPV and AIRS tracers are completely independent data sets, so that this coherent variability provides a consistency check for the relatively new AIRS data products.

[18] To further illustrate the coupling of deep convection with UTLS tracers, Figure 8 shows time series of monsoon convection proxy (OLR) together with AIRS water vapor and ozone at 350 K, averaged over the central monsoon region (20°–30°N, 60°–120°E), during May to September. The 10–20 day variability in convection is clearly evident in the water vapor data, with correlated maxima evident during the mature monsoon phase. For ozone, there is a significant drop with the onset of the monsoon in June, followed by relatively small variations associated with the convective events (phased such that ozone decreases in association with deep convection). The different behavior of water vapor and ozone in the upper troposphere following deep convection reflects the relative convective source strength and background environment for each constituent, as discussed in more detail below (see also the work of *Dessler and Sherwood* [2004], who discuss similar convective influence on the lower stratosphere).

[19] We note that when the strongest deep convective events begin in late June, as the monsoon circulation becomes mature (Figure 4), water vapor abruptly increases, then remains relatively high throughout the monsoon season. Similar behavior is observed for ozone but with low values during the mature phase. During the mature phase the constituents vary coherently with convection (OLR), and after the breakdown of the anticyclone in September, they return to their premonsoon conditions.

5. Synoptic Evolution

[20] In this section we study the detailed behavior of one particular deep convective event, tracing the synoptic evolution of the monsoon circulation and constituents. Each of the events highlighted with arrows in Figure 4 are different in detail, but here we attempt to focus on features that are typical. Figure 9 shows the evolution of 360 K MPV and deep convection for July 8, 10, and 13 (following the OLR minimum over ~July 3–8 in Figure 4). The relative maximum in deep convection on July 8 (near 80°E) is associated with a local minimum in MPV. We have not performed a detailed budget analysis for PV (MPV), but the association of deep convection and local minimum MPV in the upper troposphere is consistent with PV decreasing via the vertical gradient of diabatic heating associated with deep convection [see *Andrews et al.*, 1987, equation (3.8.5)]. This region of low MPV is then advected clockwise by the anticyclonic circulation, wrapping into a spiral structure to the west of convection on July 10, followed by a ring-like structure in MPV on July 13. Both the area of low MPV and the intensity of the anticyclonic circulation have increased

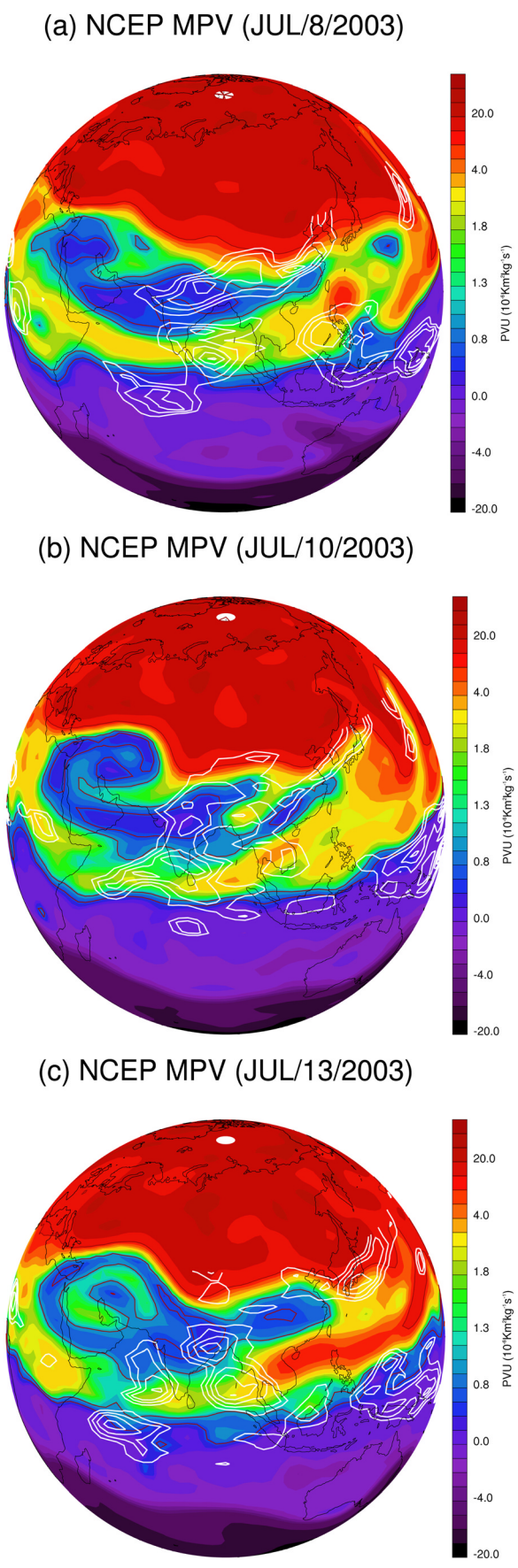

during this time (see Figure 4). Furthermore, relatively high MPV is advected around the east side of the anticyclone, forming a maximum to the southeast on July 13. This equatorward advection of high MPV is a consistent feature of the convective events, as seen in the repeated MPV maxima near 10°–20°N in Figure 7a.

[21] Figure 10a shows the circulation of the anticyclone at 100 hPa on July 10, and Figure 10b shows the corresponding structure of water vapor at 350 K. Note that for this day the circulation is particularly strong on the western side of the anticyclone, and this corresponds to the wrapped local MPV minima seen in Figure 9b. The water vapor structure in Figure 10b shows an overall maximum within the anticyclone (denoted by the 14,320 m 150 hPa geopotential contour in Figure 10b), and furthermore exhibits approximate correlation with MPV; note especially that the spiral structure in MPV (Figure 9b) is evident in the water vapor measurements. This behavior, together with the strong temporal coupling of convection and water vapor seen in Figure 8, is consistent with deep convection being a source of both low MPV and high water vapor, which are subsequently advected similarly by the anticyclonic circulation.

[22] Ozone behaves in a similar overall manner to water vapor (with anomalies of opposite sign), but the background gradients give rise to different behavior. Figure 11 shows AIRS ozone on July 13, revealing low ozone within the anticyclone. Note there is a tongue of high ozone on the southeastern edge of the anticyclone that has been advected by the circulation in a manner similar to the MPV field in Figure 9c. As with MPV, this is a characteristic feature of ozone variability associated with deep convection and enhanced anticyclonic circulation (note the corresponding episodic ozone dipole patterns in Figure 7c). This circulation and transport on the eastern edge of the anticyclone is also evident for the North American summer monsoon, as discussed recently by *Gettelman et al.* [2004a] and *Li et al.* [2005b].

[23] To explore the vertical structure of convective influence on water vapor and ozone, we take differences of observations before and after particular events (i.e., differences between the constituent maxima and minima in Figure 8). The strongest such changes in Figure 8 occur during the onset of the mature phase of the anticyclone, near the middle of June. Note that the ozone changes are relatively large at this time, with smaller changes seen throughout the rest of the mature monsoon phase; in contrast, water vapor in Figure 8 shows large changes associated with each convective event. Figure 12 shows cross sections of percent changes in water vapor and ozone during June 15–19. Both constituents show largest changes over isentropes ~340–360 K, or altitudes near ~7–13 km; the overall water vapor changes are slightly poleward of the ozone changes, although the origin of this difference is unclear. The relative increase in water vapor over these days is above 100%, while ozone shows decreases of ~20%.

Figure 9. Synoptic evolution of MPV (PVU) at 360 K for (a) July 8, (b) July 10, and (c) July 13. White lines show corresponding variations of deep convection (OLR values $\leq$210 W m^{-2}).

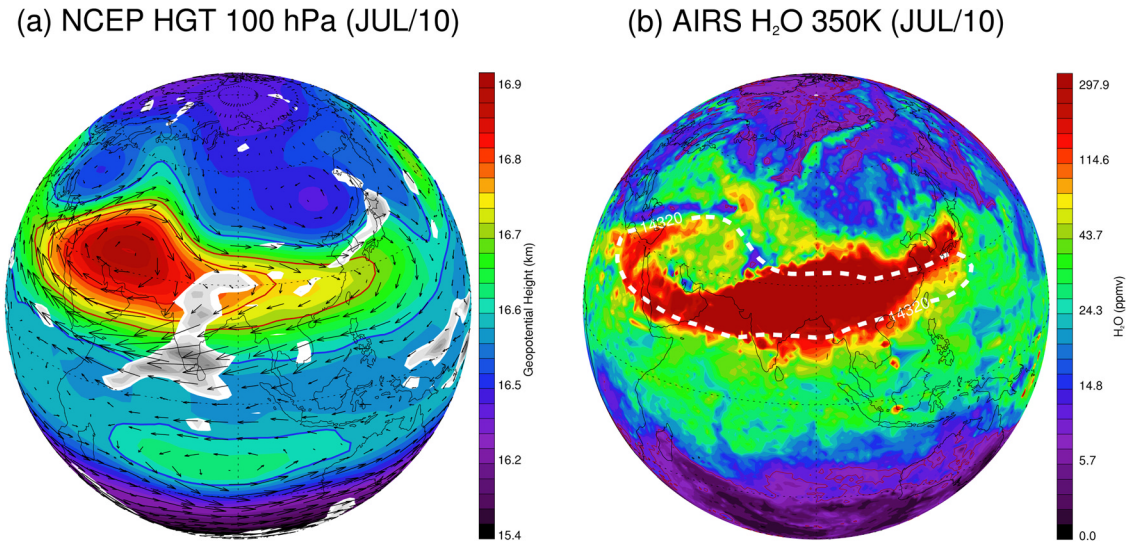

Figure 10. Map of (a) NCEP geopotential height (m) and horizontal winds (m s^{-1}) at 100 hPa and (b) AIRS water vapor (ppmv) at 350 K for July 10. The deep convective regions (OLR $\leq$ 190 Wm^{-2}) are marked by white filled contours in Figure 10a. The white dashed line in Figure 10b shows the 14,320 m geopotential height contour at 150 hPa, which is near the axis of maximum anticyclonic winds.

Figure 12 also indicates the altitude of deep convection within the monsoon region (20°–30°N) during these days (dots in Figure 12), as derived from the OLR brightness temperatures combined with the background temperature structure; this altitude is probably close to the region of detrainment for deep convection. There is reasonable agreement between the altitude of the inferred detrainment ($\sim$10 km) and the altitude of observed changes in water vapor and ozone, and we view this as a consistency check between these independent data sets. These diagnostics are consistent with episodic deep convection transporting air with high moisture and low ozone into the upper troposphere. The persistence of the constituent patterns within the monsoon region (for example, Figure 1) suggests the air is confined by the anticyclonic circulation (as discussed by *Li et al.* [2005a, 2005b]), and this is quantified below.

6. Confinement Within the Monsoon Anticyclone

[24] We investigate confinement within the monsoon anticyclone on the basis of 3-D trajectory calculations using the NCEP/NCAR wind fields, following *Bowman* [1993]. A group of 2400 particles are initialized on isobaric surfaces within the anticyclone, as shown in Figure 13a, and a series of trajectory calculations is run for 20 days. The simulations are begun every 5 days during July and August 2003, and the ensemble of runs allows estimates of transport that are not dependent on the specific starting date. Results are shown in Figures 13b and 13c for transport after 10 and 20 days, for particles initialized at 150 hPa on July 1, 2003. In both cases a majority of particles have remained within the monsoon region. For this particular case, a coherent group of particles has been advected outside and to the east of the monsoon anticyclone on day 10 (Figure 13b), but this represents a relatively small fraction of the total. This is a common feature of the calculations.

[25] The net transport out of the anticyclone can be quantified by counting the fraction of particles that remain within the boundary as a function of time. For simplicity, we choose the climatological anticyclone structure shown in Figure 13 as this boundary, taken from the time average structure shown in Figure 1 (the 14,320 m geopotential height contour of the 150 hPa level); the overall results are not sensitive to this specific choice. Figure 14a shows time evolution of the fraction of particles inside the anticyclone,

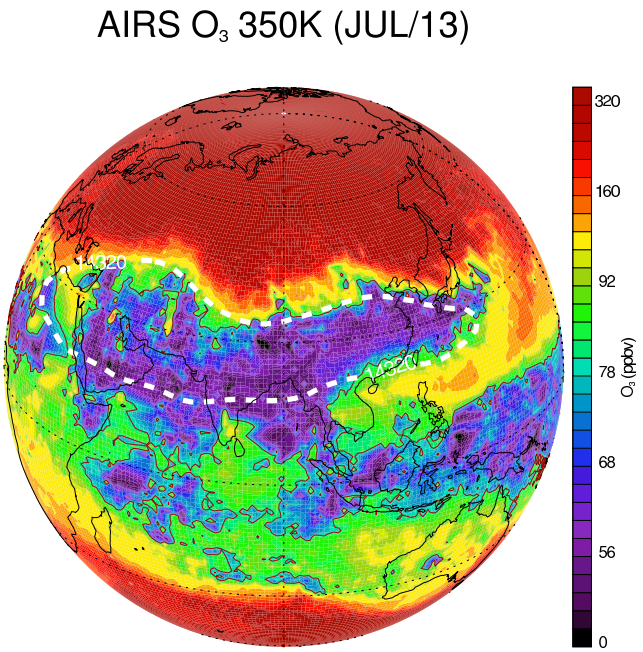

Figure 11. Synoptic map of AIRS ozone (ppbv) at 350 K with MPV (July 13). White dashed line denotes the approximate axis of maximum anticyclonic winds in the upper troposphere, as in Figure 10b.

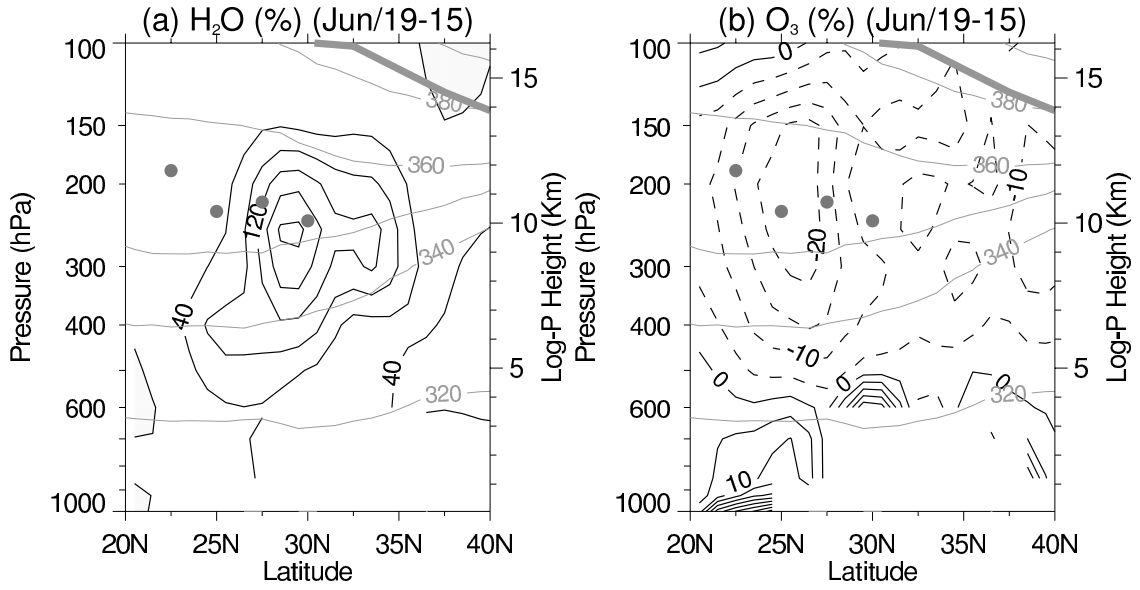

Figure 12. Percent differences in constituent mixing ratios before and after an episode of deep convection (June 15–19, 2003), for longitudes 60°–120°E, and showing results for (a) water vapor and (b) ozone, with changes in percent of the beginning value. Dots indicate estimated maximum altitude of convection over 20°–30°N, estimated from OLR data (as discussed in text).

for particles initialized at 150 hPa, for the separate calculations begun 5 days apart. For this pressure level, results show that approximately 70% of the particles remain inside the anticyclone after 10 days, and approximately 50% after 20 days. There is a relatively small spread of results from the six different starting dates, demonstrating this result is not sensitive to the specific initial conditions. These results suggest that the upper tropospheric anticyclonic circulation effectively acts to confine air for timescales of several weeks. Figure 14b shows results for similar calculations with particles initialized in the middle troposphere (400 hPa) showing much less confinement: only 40% (30%) of the particles remain inside after 10 (20) days.

[26] A summary of the vertical structure of particle confinement derived from these trajectory calculations is shown in Figure 15, derived from calculations as in Figure 14 for each pressure level (extending down to 500 hPa, although topography in this region reaches near this level, i.e., Figure 2). This shows that maximum confinement occurs in the upper troposphere, particularly over pressure levels ~200–100 hPa (~11–16 km). Note this derived structure matches the region of strongest anticyclonic winds in the monsoon region, as shown in Figure 2. Overall these transport calculations are consistent with the persistent localized water vapor and ozone structures observed in the UTLS monsoon region throughout summer (for example, Figure 1).

7. Summary and Discussion

[27] The Asian monsoon anticyclone is the dominant circulation feature in the UTLS region during Northern summer, forced by persistent deep convection coupled with the circulation [*Hoskins and Rodwell*, 1995]. The monsoon region is characterized by a warm core over the depth of the troposphere, overlaid by a cold lower stratosphere, in balance with anticyclonic winds (Figure 2) and relatively low potential vorticity (Figure 1). The monsoon is also characterized by localized extrema in UTLS constituent fields, including water vapor, ozone, methane, carbon monoxide, and other species [*Rosenlof et al.*, 1997; *Jackson et al.*, 1998; *Randel et al.*, 2001; *Park et al.*, 2004; *Li et al.*, 2005a]. *Li et al.* [2001] suggest that this circulation may also contribute to a summer tropospheric ozone maximum over the Middle East. This work has focused on understanding variability of the monsoon circulation and trace constituents during summer, including their relation to fluctuations in deep convection, and mechanisms for maintenance of the observed climatological structures.

[28] The monsoon anticyclone exhibits substantial intraseasonal oscillations, which are tied to variable forcing from transient deep convection over the Indian subcontinent and the Bay of Bengal. This variability is typically referred to as active/break cycles of the monsoon, with timescales of ~10–20 days. The daily OLR data show traveling and transient variability over the monsoon region (Figure 3), and the overall intensity of convection varies with a ~10–20 day timescale (Figure 4). The strength of the monsoon anticyclone, as diagnosed by the area of low MPV and intensity of the circulation (equation (1)), shows variations that are coherent with the convection (Figure 4). Significant correlations exist between OLR (deep convection) and temperature and circulation within the monsoon region, such that the entire balanced anticyclone varies in concert with convective heating: enhanced convection leads to warmer tropospheric temperatures, stronger anticyclonic circulation, and colder lower stratospheric (and tropopause) temperatures. The spatial patterns of temperature correlations with deep convection (Figure 6b) reveal structure consistent with a large-scale response to off-equatorial heating [e.g., *Gill*, 1980; *Dima et al.*, 2005].

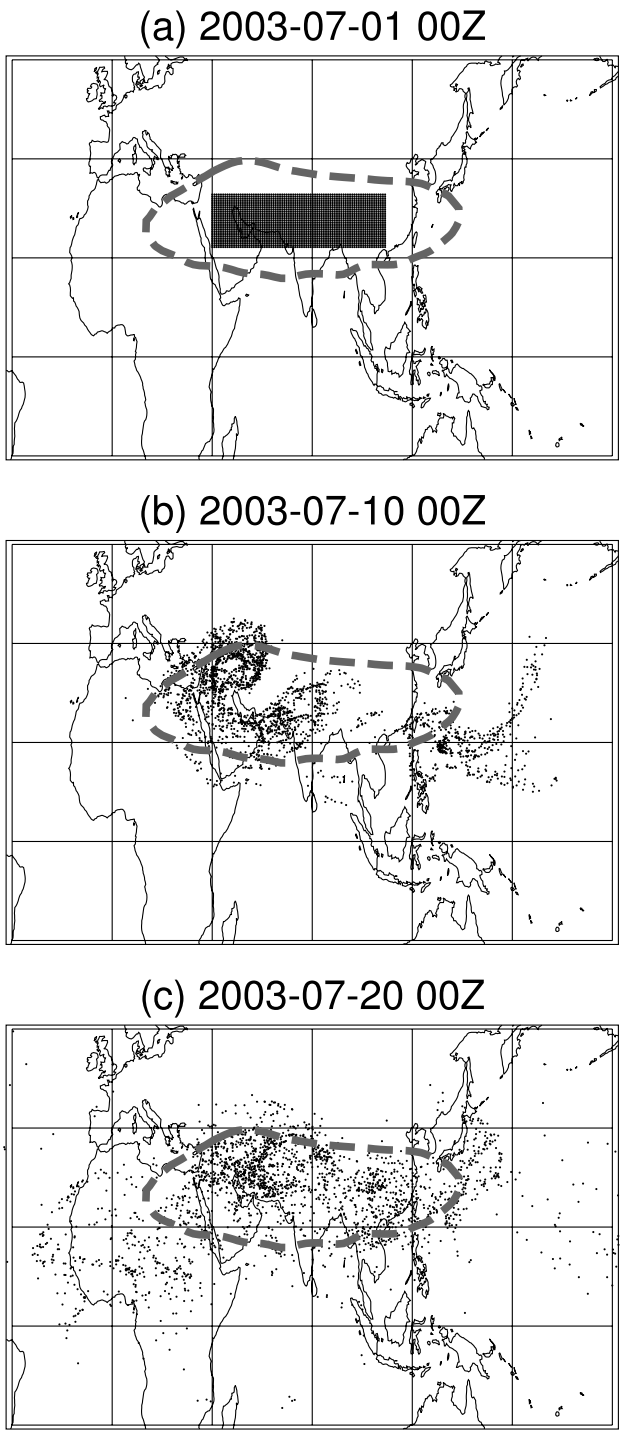

Figure 13. Map of particles initialized on the 150 hPa level on (a) July 1, 2003, and (b) after 10 days and (c) 20 days trajectory runs. Long dashed lines indicate July and August average 14,320 m geopotential height at 150 hPa (see Figure 1), which we use as a simplified boundary for the monsoon anticyclone.

[29] Upper tropospheric water vapor and ozone measured by AIRS show strong localized extrema associated with the monsoon (Figure 1). Furthermore, both the seasonal and synoptic timescale variations in water vapor and ozone exhibit variations linked to convection in the monsoon region (Figures 7 and 8). Water vapor exhibits enhanced values within the anticyclone, owing to vertical transport of moist air during deep convection. Conversely, ozone shows relatively low values within the monsoon, owing to the convective transport of air with low ozone mixing ratio from near surface levels. The direct association between the constituents and deep convection is evidenced by correlated time variations (Figure 8), and also the fact that constituent changes occur over altitudes that are consistent with outflow from deep convection (Figure 12). We note that *Dessler and Sherwood* [2004] have used idealized calculations to study convective effects on water vapor and ozone in the monsoon region, focusing on the lower stratosphere (380 K potential temperature). They find that convection has a stronger influence on water vapor than ozone in this region, because of contrasts between the convective outflow and background environment. While a similar observational result is found in the analysis here, the details of their calculations do not extend to the upper troposphere; among other things, the convective turnover time is very different between the upper troposphere and lower stratosphere.

[30] The synoptic evolution of the monsoon anticyclone following enhanced deep convection shows localized minima in MPV near the convective region, followed by

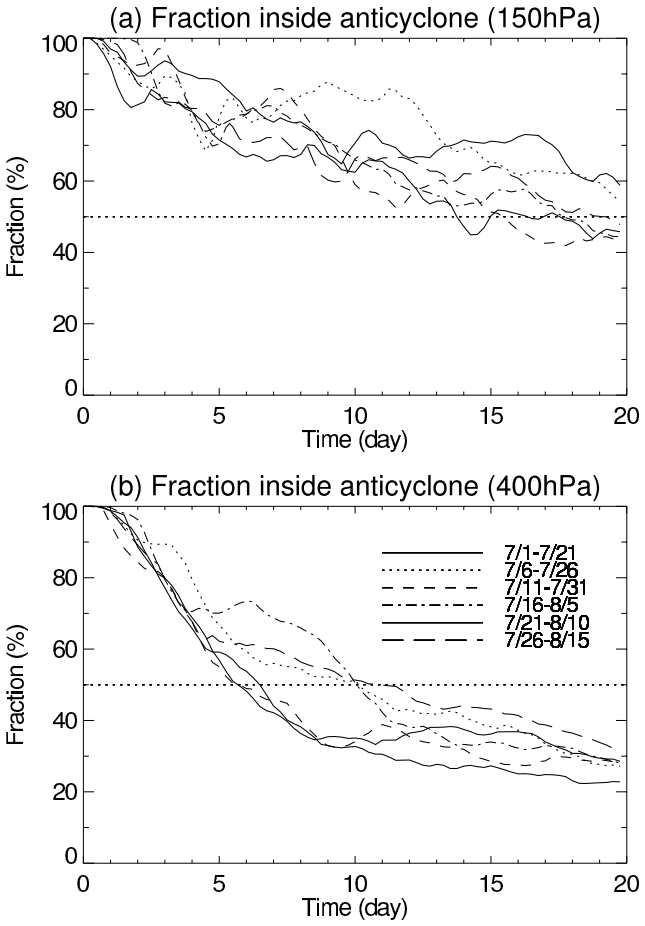

Figure 14. Time series of fraction of particles inside anticyclone for six trajectory simulations during July and August 2003 (each run starts 5 days apart). Results are shown for particles initialized at (a) 150 hPa and (b) 400 hPa.

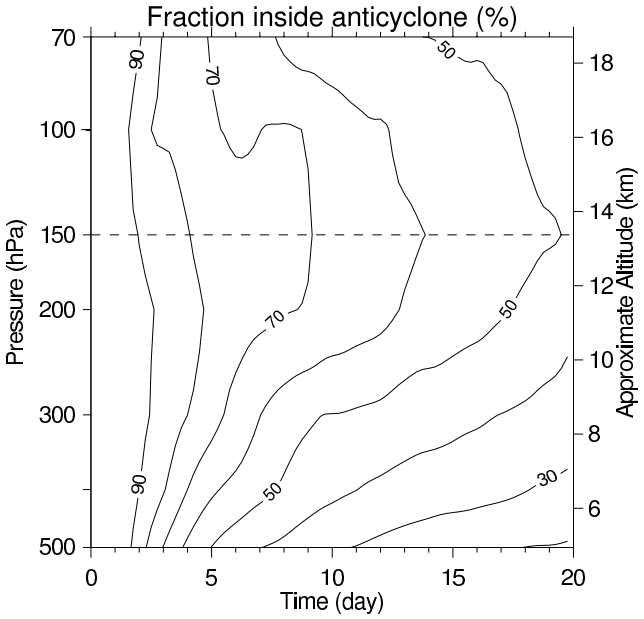

Figure 15. Fraction of particles inside the anticyclone as a function of pressure level and time, derived from the ensemble of transport calculations (as in Figure 14).

anticyclonic advection which can result in a wrapping up of MPV to the west of convection, or even a ring-like structure spanning the anticyclone (Figure 9). These variations in MPV can also be observed in water vapor (Figure 10), and in general there can be reasonable synoptic correlation between these fields. The enhanced anticyclonic circulation is also associated with strong equatorward advection on the eastern flank of the anticyclone, with regions of high MPV and low ozone characteristic of stratospheric air brought to low latitudes (Figures 9c and 11). The result is a region of reversed meridional gradients on the eastern side of the anticyclone, and these occur repeatedly during summer in response to enhanced convection (Figure 7). We note this is a region of chronic Rossby-wave breaking, as identified by reversed PV gradients [*Postel and Hitchman*, 1999].

[31] The persistence of the constituent patterns within the monsoon region, together with the climatological wind structure (Figure 2), suggests that air is confined by the UTLS anticyclonic circulation. We have studied this confinement using idealized transport calculations for particles initialized on individual pressure levels within the anticyclone. Results show that the anticyclone can confine a large fraction of particles initialized in the upper troposphere for timescales of several weeks, whereas particles in the middle troposphere or lower stratosphere disperse more quickly (Figures 13–15). The maximum confinement occurs over pressure levels ~200–100 hPa, and this agrees qualitatively with the vertical structure of the strongest monsoon winds (Figure 2). While these are idealized calculations and more systematic studies should be pursued, the results suggest that dynamical confinement within the anticyclone is an important component of understanding the structure of constituents in the monsoon region.

[32] **Acknowledgments.** This work was partially supported by the Korea Research Foundation grant funded by the Korean Government (MOEHRD) (C00123) and by grants from the NASA ACMAP and EOS programs. We thank Andrew Gettelman for constructing the gridded AIRS data sets and for discussions throughout the course of this work, and we thank Ken Bowman for the use of his trajectory code and a constructive review of the manuscript. We also thank Roland Garcia, Jonathan Jiang, J.-F. Lamarque, Qinbin Li, and Dong Wu for discussions and comments on the manuscript. The National Center for Atmospheric Research is operated by the University Corporation for Atmospheric Research, under sponsorship of the National Science Foundation.

References

Andrews, D. G., J. R. Holton, and C. B. Leovy (1987), *Middle Atmosphere Dynamics*, 489 pp., Elsevier, New York.

Annamalai, H., and J. M. Slingo (2001), Active/break cycles: Diagnosis of the intraseasonal variability of the Asian summer monsoon, *Clim. Dyn.*, *18*, 85–102.

Aumann, H. H., et al. (2003), AIRS/AMSU/HSB on the Aqua Mission: Design, science objectives and data products, *IEEE Trans. Geosci. Remote Sens.*, *41*, 253–264.

Bannister, R. N., A. O'Neill, A. R. Gregory, and K. M. Nissen (2004), The role of the south-east Asian monsoon and other seasonal features in creating the 'tape-recorder' signal in the Unified Model, *Q. J. R. Meteorol. Soc.*, *130*, 1531–1554.

Bowman, K. P. (1993), Large-scale isentropic mixing properties of the Antarctic polar vortex from analyzed winds, *J. Geophys. Res.*, *98*, 23,013–23,027.

Bowman, K. P. (2006), Transport of carbon monoxide from the tropics to the extratropics, *J. Geophys. Res.*, *111*, D02107, doi:10.1029/2005JD006137.

Dessler, A. E., and S. C. Sherwood (2004), Effect of convection on the summertime extratropical lower stratosphere, *J. Geophys. Res.*, *109*, D23301, doi:10.1029/2004JD005209.

Dethof, A., A. O'Neill, J. M. Slingo, and H. G. J. Smit (1999), A mechanism for moistening the lower stratosphere involving the Asian summer monsoon, *Q. J. R. Meteorol. Soc.*, *125*, 1079–1106.

Dima, I. M., J. M. Wallace, and I. Kraucunas (2005), Tropical zonal momentum balance in the NCEP reanalyses, *J. Atmos. Sci.*, *62*, 2499–2513.

Efron, B., and R. J. Tibshirani (1993), *An Introduction to the Bootstrap*, 436 pp., CRC Press, Boca Raton, Fla.

Fujinami, H., and T. Yasunari (2004), Submonthly variability of convection and circulation over and around the Tibetan Plateau during the boreal summer, *J. Meteorol. Soc. Japan*, *82*, 1545–1564.

Gettelman, A., D. E. Kinnison, T. J. Dunkerton, and G. P. Brasseur (2004a), Impact of monsoon circulations on the upper troposphere and lower stratosphere, *J. Geophys. Res.*, *109*, D22101, doi:10.1029/2004JD004878.

Gettelman, A., et al. (2004b), Validation of Aqua satellite data in the upper troposphere and lower stratosphere with in situ aircraft instruments, *Geophys. Res. Lett.*, *31*, L22107, doi:10.1029/2004GL020730.

Gill, A. E. (1980), Some simple solutions for heat-induced tropical circulation, *Q. J. R. Meteorol. Soc.*, *106*, 447–462.

Hagan, D. E., C. R. Webster, C. B. Farmer, R. D. May, R. L. Herman, E. M. Weinstock, L. E. Christensen, L. R. Lait, and P. A. Newman (2004), Validating AIRS upper atmosphere water vapor retrievals using aircraft and balloon in situ measurements, *Geophys. Res. Lett.*, *31*, L21103, doi:10.1029/2004GL020302.

Haynes, P., and E. Shuckburgh (2000), Effective diffusivity as a diagnostic of atmospheric transport, 2, Troposphere and lower stratosphere, *J. Geophys. Res.*, *105*, 22,795–22,810.

Highwood, E. J., and B. J. Hoskins (1998), The tropical tropopause, *Q. J. R. Meteorol. Soc.*, *124*, 1579–1604.

Holton, J. R. (2004), *An Introduction to Dynamic Meteorology*, 4th ed., 535 pp., Elsevier, New York.

Hoskins, B. J., and M. J. Rodwell (1995), A model of the Asian summer monsoon, I, The global scale, *J. Atmos. Sci.*, *52*, 1329–1340.

Hsu, C. J., and R. A. Plumb (2000), Nonaxisymmetric thermally driven circulations and upper-tropospheric monsoon dynamics, *J. Atmos. Sci.*, *57*, 1255–1276.

Jackson, D. R., S. J. Driscoll, E. J. Highwood, J. E. Harries, and J. M. Russell III (1998), Troposphere to stratosphere transport at low latitudes as studied using HALOE observations of water vapour 1992–1997, *Q. J. R. Meteorol. Soc.*, *124*, 169–192.

Kalnay, E., et al. (1996), The NCEP/NCAR 40-year reanalysis project, *Bull. Am. Meteorol. Soc.*, *77*, 437–471.

Krishnamurti, T. N., and P. Ardanuy (1980), The 10 to 20-day westward propagating mode and "Breaks in the Monsoons", *Tellus*, *32*, 15–26.

Krishnamurti, T. N., and H. H. Bhalme (1976), Oscillations of a monsoon system, I, Observational aspects, *J. Atmos. Sci.*, *33*, 1937–1954.

Lait, L. R. (1994), An alternative form for potential vorticity, *J. Atmos. Sci.*, *51*, 1754–1759.

Li, Q., et al. (2001), A tropospheric ozone maximum over the Middle East, *Geophys. Res. Lett.*, *28*, 3235–3238.

Li, Q., et al. (2005a), Convective outflow of South Asian pollution: A global CTM simulation compared with EOS MLS observations, *Geophys. Res. Lett.*, *32*, L14826, doi:10.1029/2005GL022762.

Li, Q., D. J. Jacob, R. Park, Y. Wang, C. L. Heald, R. Hudman, R. M. Yantosca, R. V. Martin, and M. Evans (2005b), North American pollution outflow and the trapping of convectively lifted pollution by upper-level anticyclone, *J. Geophys. Res.*, *110*, D10301, doi:10.1029/2004JD005039.

Liebman, B., and C. A. Smith (1996), Description of a complete (interpolated) outgoing longwave radiation dataset, *Bull. Am. Meteorol. Soc.*, *77*, 1275–1277.

Park, M., W. J. Randel, D. E. Kinnison, R. R. Garcia, and W. Choi (2004), Seasonal variation of methane, water vapor, and nitrogen oxides near the tropopause: Satellite observations and model simulations, *J. Geophys. Res.*, *109*, D03302, doi:10.1029/2003JD003706.

Popovic, J. M., and R. A. Plumb (2001), Eddy shedding from the upper-tropospheric Asian monsoon anticyclone, *J. Atmos. Sci.*, *58*, 93–104.

Postel, G. A., and M. H. Hitchman (1999), A climatology of Rossby waves breaking along the subtropical tropopause, *J. Atmos. Sci.*, *56*, 359–373.

Randel, W. J., F. Wu, A. Gettelman, J. M. Russell III, J. M. Jawodny, and S. J. Oltmans (2001), Seasonal variation of water vapor in the lower stratosphere observed in Halogen Occultation Experiment data, *J. Geophys. Res.*, *106*, 14,313–14,325.

Renka, R. (1982), *Interpolation of Data on the Surface of a Sphere*, *Rep. ORNL/CSD-108*, Oak Ridge Natl. Lab., Oak Ridge, Tenn.

Rosenlof, K. H., A. F. Tuck, K. K. Kelly, J. M. Russell III, and M. P. McCormick (1997), Hemispheric asymmetries in water vapor and inferences about transport in the lower stratosphere, *J. Geophys. Res.*, *102*, 13,213–13,234.

Wang, P.-H., P. Minnis, M. P. McCormick, G. S. Kent, and K. M. Skeens (1996), A 6–year climatology of cloud occurrence frequency from Stratospheric Aerosol and Gas Experiment II observations (1985–1990), *J. Geophys. Res.*, *101*, 29,407–29,430.

Yasunari, T. (1981), Structure of an Indian summer monsoon system with a period around 40–days, *J. Meteorol. Soc. Jpn.*, *59*, 336–354.

M. Park and W. J. Randel, National Center for Atmospheric Research, P.O. Box 3000, Boulder, CO 80307-3000, USA. (mijeong@ucar.edu; randel@ucar.edu)